AGU
ADVANCING
EARTH AND
SPACE SCIENCES

Earth's Future

Key Points:

- We present a database of 7,764 reported large (A ≥ 0.1 km^2) slow-moving landslides in nine IPCC regions and find 563 are inhabited
- We learn more about landslide exposure from regional responses to flood exposure than from an abundance of slow-moving landslides
- Urbanization in basins can be a relevant driver of landslide exposure, while steepness and flood exposure have varying regional influences

Human Settlement Pressure Drives Slow-Moving Landslide Exposure

Joaquin V. Ferrer[1,2] ⓘ, Guilherme Samprogna Mohor[1] ⓘ, Olivier Dewitte[3] ⓘ, Tomáš Pánek[4] ⓘ, Cristina Reyes-Carmona[5,6] ⓘ, Alexander L. Handwerger[7,8] ⓘ, Marcel Hürlimann[9] ⓘ, Lisa Köhler[1,10] ⓘ, Kanayim Teshebaeva[11] ⓘ, Annegret H. Thieken[1] ⓘ, Ching-Ying Tsou[12] ⓘ, Alexandra Urgilez Vinueza[13] ⓘ, Valentino Demurtas[14] ⓘ, Yi Zhang[15] ⓘ, Chaoying Zhao[16] ⓘ, Norbert Marwan[2] ⓘ, Jürgen Kurths[2] ⓘ, and Oliver Korup[1] ⓘ

[1]Institute of Environmental Sciences and Geography, University of Potsdam, Potsdam-Golm, Germany, [2]Potsdam Institute for Climate Impact Research, Member of the Leibniz Association, Postdam, Germany, [3]Department of Earth Sciences, Royal Museum for Central Africa, Tervuren, Belgium, [4]Department of Physical Geography and Geoecology, University of Ostrava, Ostrava, Czech Republic, [5]Department of Earth and Environmental Sciences, University of Milano-Bicocca, Milan, Italy, [6]Department of Civil Engineering, University of Alicante, Alicante, Spain, [7]Jet Propulsion Laboratory, California Institute of Technology, Pasadena, CA, USA, [8]Joint Institute for Regional Earth System Science and Engineering, University of California, Los Angeles, Los Angeles, CA, USA, [9]Department of Civil and Environmental Engineering, UPC BarcelonaTECH, Barcelona, Spain, [10]Department of Urban and Environmental Sociology, Helmholtz-Centre for Environmental Research-UFZ Leipzig, Leipzig, Germany, [11]GFZ German Research Center for Geosciences, Potsdam, Germany, [12]Faculty of Agriculture and Life Science, Hirosaki University, Hirosaki, Japan, [13]Water Management Department, Delft University of Technology, Delft, The Netherlands, [14]Department of Chemical and Geological Sciences, University of Cagliari, Monserrato, Italy, [15]School of Earth Sciences, Lanzhou University, Lanzhou, China, [16]School of Geological Engineering and Geomatics, Chang'an University, Chang'an, China

Abstract A rapidly growing population across mountain regions is pressuring expansion onto steeper slopes, leading to increased exposure of people and their assets to slow-moving landslides. These moving hillslopes can inflict damage to buildings and infrastructure, accelerate with urban alterations, and catastrophically fail with climatic and weather extremes. Yet, systematic estimates of slow-moving landslide exposure and their drivers have been elusive. Here, we present a new global database of 7,764 large (A ≥ 0.1 km^2) slow-moving landslides across nine IPCC regions. Using high-resolution human settlement footprint data, we identify 563 inhabited landslides. We estimate that 9% of reported slow-moving landslides are inhabited, in a given basin, and have 12% of their areas occupied by human settlements, on average. We find the density of settlements on unstable slopes decreases in basins more affected by slow-moving landslides, but varies across regions with greater flood exposure. Across most regions, urbanization can be a relevant driver of slow-moving landslide exposure, while steepness and flood exposure have regionally varying influences. In East Asia, slow-moving landslide exposure increases with urbanization, gentler slopes, and less flood exposure. Our findings quantify how disparate knowledge creates uncertainty that undermines an assessment of the drivers of slow-moving landslide exposure in mountain regions, facing a future of rising risk, such as Central Asia, Northeast Africa, and the Tibetan Plateau.

Plain Language Summary Slow-moving landslides can damage buildings and infrastructure, while potentially leading to thousands of fatalities with a sudden collapse. As populations expand in mountain regions, more communities settling into steeper terrain could be exposed to landslide-prone areas. Yet, our estimates of populations exposed to landslides excludes slow-moving landslides. We address this by identifying unstable slopes, inhabited by human settlements, from a new global database of 7,764 reported large slow-moving landslides located in nine IPCC mountain-risk regions. Across most regions, we find that landslide exposure increases with sprawling urbanized areas, though clearly not with steeper terrain. We show regional contrasts in how exposure to floods may drive people to settle on unstable slopes. East Asia stands out in how landslide exposure increases in more urbanized basins with gentler slopes and less flood exposure. Our results indicate that communities in mountain regions, facing increasing future landslide and flood risk, have the least certain insight on slow-moving landslide exposure and their drivers.

Supervision: Norbert Marwan, Jürgen Kurths, Oliver Korup
Validation: Joaquin V. Ferrer, Guilherme Samprogna Mohor, Oliver Korup
Visualization: Cristina Reyes-Carmona
Writing – original draft: Joaquin V. Ferrer, Guilherme Samprogna Mohor, Olivier Dewitte, Tomáš Pánek, Cristina Reyes-Carmona, Alexander L. Handwerger, Marcel Hürlimann, Kanayim Teshebaeva, Annegret H. Thieken, Ching-Ying Tsou, Alexandra Urgilez Vinueza, Norbert Marwan, Jürgen Kurths, Oliver Korup
Writing – review & editing: Joaquin V. Ferrer, Guilherme Samprogna Mohor, Olivier Dewitte, Tomáš Pánek, Cristina Reyes-Carmona, Alexander L. Handwerger, Marcel Hürlimann, Kanayim Teshebaeva, Annegret H. Thieken, Ching-Ying Tsou, Alexandra Urgilez Vinueza, Valentino Demurtas, Yi Zhang, Chaoying Zhao, Norbert Marwan, Jürgen Kurths, Oliver Korup

1. Introduction

The world's rapidly rising and expanding population, together with migration and contemporary climate change, are significantly contributing to increased landslide and flood risk for 1.28 billion people across mountain regions (Adler et al., 2022). More than half of the global population is urban (United Nations, Department of Economic and Social Affairs, Population Division, 2019) and up to 40% of the mountain population in cities (Thornton et al., 2022). People are pulled toward a promise of better livelihoods in cities, while pushed away from rural mountain regions by conflict and environmental degradation (Bachmann et al., 2019). Amid limited terrain suitable for settlements (Omurakunova et al., 2020; Rusk et al., 2022; Shi et al., 2023), communities may need to opt for a compromise in hazard avoidance, with damaging floods capable of driving settlements away from rivers (Mård et al., 2018) and onto hillslopes prone to landslides (Gong et al., 2021).

In steep terrain, many slopes that appear amenable to human settlements may host slow-moving landslides (Cignetti et al., 2023; Forno et al., 2013; Reyes-Carmona et al., 2023). These landslides are mass movements of coherent soil and rock moving along discrete shear zones (Hungr et al., 2014; Lacroix et al., 2020; Mansour et al., 2011) and can involve entire continuously deforming hillslopes (Cignetti et al., 2023; Pánek & Klimeš, 2016). Slow-moving landslides that claim lives are rare (Lacroix et al., 2020) and communities may find benefit in expanding uphill despite the landslide risk present (Depicker et al., 2021; Maki Mateso et al., 2024; Tuladhar et al., 2015). Their motion inflicts damage to buildings and infrastructure (Mansour et al., 2011) and can culminate in catastrophic failure (Handwerger, Huang, et al., 2019; Pánek & Klimeš, 2016). The associated costs and risks can be substantial, but remain cursorily documented. For example, slow-moving landslides in the Tena Valley, Central Spanish Pyrenees, cost € 15 million to roads two decades ago (Herrera et al., 2013), while € 7 billion in assets are presently at risk in the Arno River basin, Italy (Caleca et al., 2022). Abrupt accelerations and movements of slow-moving landslides can require evacuation or even abandonment and resettlement (Bellas & Voulgaridis, 2018; Gizzi et al., 2019; Solari et al., 2018). In 2023, an abrupt subsidence of a landslide beneath the towns of Joshimath and Bhatwari (~20,000 inhabitants) in Uttarakhand, India, required an evacuation (Sundriyal et al., 2023).

The influence of climate change on processes governing movements of large landslides is difficult to ascertain. The changes in surface and subsurface hydrology that accompany an urbanization of slopes could accelerate slow-moving landslides (Dille et al., 2022; Lacroix et al., 2020; Notti et al., 2015). They may further accelerate in response to seasonal rainfall (Emberson et al., 2021; Handwerger et al., 2022; Handwerger, Huang, et al., 2019), or even atmospheric pressure fluctuations (Pelascini et al., 2022; Schulz et al., 2009). Moreover, shifts from dry-to-wet extremes could lead to rapid acceleration of some of these slopes (Handwerger, Fielding, et al., 2019), imposing greater risk in the future to exposed communities and their infrastructure.

While these examples highlight potentially adverse consequences from exposure to slow-moving landslides, our current insight rests more on lessons learned than on proactive assessments. Hence, a global overview of slow-moving landslide exposure remains elusive. Most exposure assessments at present focus on fast-moving landslides associated to climatic (Haque et al., 2019; Lin et al., 2023) or earthquake triggers (Nadim et al., 2006), but exclude slow-moving landslides (Emberson et al., 2020, 2021). Importantly, this generates an uncertain degree of risk in regions with growing populations exposed to rising landslide and flood hazards (Adler et al., 2022).

Here, we systematically assess the global and regional exposure to large slow-moving landslides affecting at least 0.1 km^2; we refer to these simply as landslides. We estimate the occupation status of landslides in our new global database (containing landslides with reported deformations rates from 1 mm y^{-1} to 3 m y^{-1}) using high-resolution human settlement data (Marconcini et al., 2020). Our results aim to inform policy and governance processes with a first estimate of slow-moving landslide exposure and their potential drivers, aggregated at basin-scale. To this extent, we located basins with slow-moving landslides in IPCC regions, representing climatic consistency harmonized with models projecting future scenarios (Iturbide et al., 2020), that were assessed for projected climate-driven risk from flood and landslide hazards affecting growing populations in mountain regions (Adler et al., 2022).

We introduce concepts of landslide exposure at the drainage basin-level as the fraction of inhabited landslides (Figure 1a) and density to which landslides are inhabited with the relative area of settlements present on a given landslide (Figure 1b). We further derive insight on the drivers of the extent of human settlements inhabiting landslides, using the linear responses between the relative areas of settlements on landslides to an abundance of
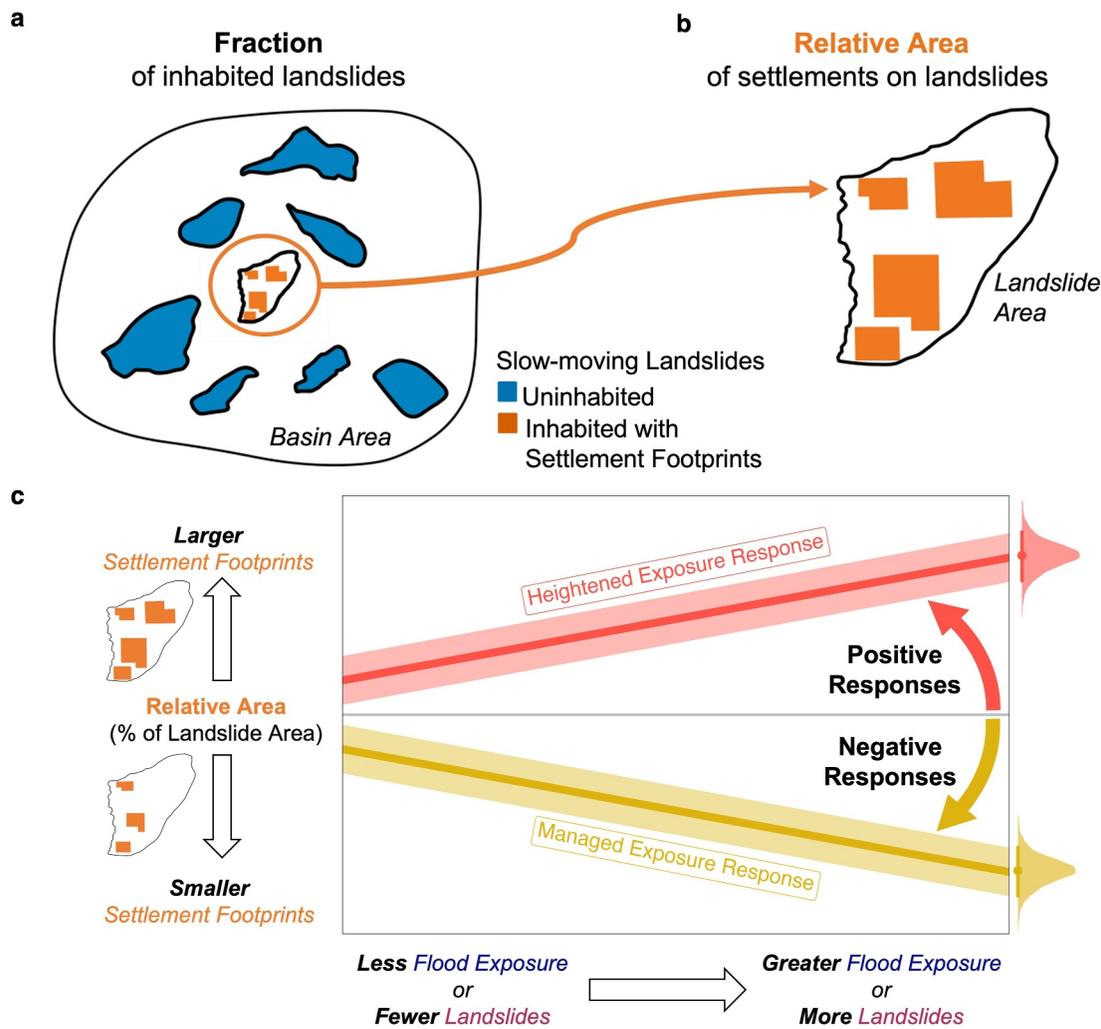
Figure 1. Concepts of exposure to slow-moving landslides. (a) Exposure measured by the fraction of inhabited landslides that sustain human settlements. (b) Relative area of human settlement footprints on a given landslide. (c) Possible relationship of relative landslide area inhabited (% of landslide area) with greater fractions of a basin exposed to floods and or affected by landslides (% of basin area). The two lines show possible linear responses of settlement footprints to flood exposure and more landslides; probability distributions on the right show the range possible of either linear trend.

slow-moving landslides, or the level flood exposure in basins across IPCC regions. We interpret *heightened exposure* from positive linear responses to the basin area affected by either hazard, while *managed exposure* from negative ones (Figure 1c). Finally, we investigate regional influences of basin characteristics in predicting the patterns of human settlements on landslides using the fraction of area urbanized, average slope steepness, and the fraction of flood-exposed area.

2. Data and Methods

2.1. Compiling a Global Database of Slow-Moving Landslides

We systematically assessed the global and regional exposure of settlements on large slow-moving landslides affecting areas ≥ 0.1 km^2; we refer to these simply as landslides. Our new global geodatabase is a compilation of 7,764 large slow-moving landslides identified by reported deformation rates (ranging from 1 mm y^{-1} to 3 m y^{-1}), and slope failures labeled as "active" or labeled as a "deep-seated gravitational slope deformation" (DSGSDs) (Demurtas et al., 2021; Hungr et al., 2014; Pánek & Klimeš, 2016) in the original publications. This database of landslides is a compilation of mapped landslide areas taken from 40 sources (Table S1 in Supporting Information S1); these are open-access databases (17), journal articles with inventories obtained via correspondence (24), and published maps that we digitized (9). We include slow-moving landslides with movements in the range of

millimeters to meters per year that can damage buildings and infrastructure established on their surfaces (Mansour et al., 2011). These landslides represent areas of significant hazard from fatal and destructive debris flows that can initiate from the landslide bodies, or rapid failure following sudden accelerations (Lacroix et al., 2020). Furthermore, very slow-moving DSGSDs that involve entire hillslopes are areas that have been precursors for many of the largest catastrophic rock avalanches (Chigira et al., 2013; Pánek & Klimeš, 2016). In compiling this database, we modified some of the original shapefiles, after quality checks in consultation with local researchers, to remove redundant or spuriously overlapping polygons. We provide information from our database on available classifications of slow-moving landslide types, states of activity, and measured rates of deformation with Table S1 in Supporting Information S1.

2.2. Estimating the Exposure of Human Settlements on Slow-Moving Landslides

Landslides in our database are primarily located in mountain regions that may have sparse or low population densities. We estimated the exposure of rural settlements on slow-moving landslides in regions that may be eluded by urban footprint extent data. To this end, we used data from the World Settlement Footprint 2015 (*WSF2015*) that estimates human-occupied land with 10 m resolution, thus also including settlements in rural and suburban areas (Marconcini et al., 2020). Though, coverage is limited to permanent structures and excludes small or temporary structures with light building materials such as nomadic or refugee camps. The *WSF2015* data product has been validated by crowd sourcing and offers improved coverage compared to similar previous products.

We intersected our global database of landslides with *WSF2015* data to estimate how densely occupied each landslide was with permanent structures, measure the relative area of landslides with human settlements (Figure 1b), and identify those landslides that are inhabited. Hence, we identified inhabited landslides considering only those with $\geq 1\%$ of their area inhabited, or with settlement footprints $\geq 10,000$ m^2.

2.3. Drainage Basin Characteristics

We aggregated our analysis at the scale of drainage basins and located the slow-moving landslides in basins from the BasinATLAS database, version 10, which is a subset product of the HydroATLAS database (Lehner et al., 2022; Linke et al., 2019). The HydroATLAS provides high spatial resolution hydro-environmental information for watersheds at a global scale. The BasinATLAS database derives sub-basin characteristics from hierarchically nested watersheds at 12 spatial scales. We used drainage basins from level 10 to have sufficient basin areas for containing all slow-moving landslide areas from our database.

We estimated slow-moving landslide exposure in terms of the fraction of landslides inhabited in a basin (Figure 1a) to give context of the hydro-environmental characteristics and investigate where human settlements locate onto landslides. Within these basins, we investigated the influence characteristics on landslide exposure, taking the fraction of area urbanized, average slope steepness, density of slow-moving landslides, and fraction of flood-exposed area as predictors. The predictor variables in our analysis utilized descriptors of mean steepness, flood exposure, slow-moving landslide density, and degree of urbanization. We characterized the steepness of each basin by using the mean slopes (in degrees) from the HydroATLAS. The slopes were originally computed from a 3 arc-second digital elevation model (Robinson et al., 2014), and aggregated into a 15 arc-second resolution in the HydroATLAS database.

We further derived a flood exposure characteristic from inundation data (Fluet-Chouinard et al., 2015) to describe the extent of areas affected in a basin that may be unsuitable for establishing permanent structures. We took the spatial average of inundation extent within a basin, using monthly observations between 1994 and 2003 from the HydroATLAS, and computed a proxy for flood exposure by taking the difference between annual minima and the 12-year maximum inundation extent. However, this data is based on observations from 1993 to 2004, and is unlikely to fully cover extreme and rare flood events (Dryden et al., 2021). We conducted an additional analysis to compare the influence of basin-wide flood exposure derived from areas inundated (Fluet-Chouinard et al., 2015) and floodplain areas identified (Nardi et al., 2019) on the relative areas of landslides inhabited (Text S1 in Supporting Information S1). We selected an inundation-derived flood exposure characterization in basins to include coastal flood effects, acknowledging that high return period floods may not be captured by the inundation data (Dryden et al., 2021).

Furthermore, we calculated the fraction of the total *WSF2015* settlement footprint area per unit basin area to express the degree of urbanization. Finally, we further calculated a fraction total area with landslides per unit basin area to express slow-moving landslide density; we refer to this simply as landslide density.

2.4. Bayesian Hierarchical Modeling

Our objective was to assess slow-moving landslide exposure and identify possible drivers at the basin-scale. Hence, each landslide was assigned to a basin, with predictor variables aggregated at a basin-scale. To this end, our study not just considers areas affected by slow-moving landslides, but the basins in which they are situated, thus, incorporating areas that are also unaffected. Basins in our study were labeled with IPCC regions (Adler et al., 2022; Iturbide et al., 2020) that served as groups for our hierarchical models. We incorporated projected levels of risk to people and infrastructure from landslides and floods across mountain regions of the IPCC regions. The projections of climate-related hazards in scenarios beyond 1.7° were assessed to lead to growing risk across nearly all mountain regions (Adler et al., 2022). Hence, we labeled the regions in our study by changing risk levels beyond a threshold of 1.7°.

We assessed the exposure to slow-moving landslides across IPCC regions by modeling both the fraction of inhabited landslides in basins and the relative area of those inhabited by human settlements. We implemented our models in a Bayesian hierarchical approach (Gelman, 2006; Gelman & Hill, 2006; McElreath, 2018), where individual IPCC regions serve as labeled levels for groups of data. We numerically approximated the posterior distributions using a Hamiltonian Monte Carlo algorithm implemented in STAN (S. D. Team, 2023) and a No-U-Turn Sampler (NUTS) within the software package *brms* (Bürkner, 2017) implemented in the *R* statistical computing language (RC Team, 2023).

First, the relative area, representing the fraction of the landslide area with settlement footprints, can conventionally be modeled with a beta distribution (Ferrari & Cribari-Neto, 2004), which is defined on the unit interval and thus suitable for modeling proportions. We considered a zero-inflated variant, however, because the relative areas we estimated with the *WSF2015* data had many zero values, with only 7% of landslides in our database inhabited (Figure 2). Hence, we assume that human settlements on slow-moving landslides are rare and expect this surplus of zero-values. To account for this distortion, we used a Zero-Inflated Beta (BEZI) distribution (Ospina & Ferrari, 2010) to overcome the limitations of the beta distribution and account for excess zeros in our data with a Bernoulli distribution. This approach has been successful in predicting ratios of data with dominant zero-values (B. Tang et al., 2023; Schoppa et al., 2020). The combination of distributions has the following cumulative distribution function (CDF):

$$\text{BEZI}(y|\gamma, \mu, \phi) = F_{Bernoulli}(y|\gamma) + F_{Beta}(y > 0|\mu, \phi) \tag{1}$$

where y is the response, relative area, $F_{Bernoulli}(y|\gamma)$ is the CDF of the Bernoulli distribution with the parameter γ. $F_{Beta}(y > 0|\mu, \phi)$ is the CDF of the beta distribution for y response variables greater than zero. The beta distribution is reparametrized here such that μ_i and ϕ_i are its mean and precision parameters (Ferrari & Cribari-Neto, 2004).

We hypothesize that predictors of basin-level characteristics on exposure vary across IPCC regions. Hence, we model regional effects with partial pooling in a hierarchical model to derive models and gain regional insight while informing a pooled model across all regions. We addressed the imbalance of samples across IPCC regions in our database (Figure 2) by implementing our BEZI models with a hierarchical Bayesian model (Gelman, 2006; Gelman & Hill, 2006; McElreath, 2018):

$$Y_i \sim \text{BEZI}(\gamma_i, \mu_i, \phi_i) \tag{2}$$

where Y_i is response variable for the observation i (i.e., the relative extent of occupancy on a landslide in a basin, i). The parameter γ of the Bernoulli distribution is the conditional zero-inflation probability (i.e., the probability that the response is 0). When $Y_i > 0$, the mean μ of the beta distribution is estimated alongside the precision parameter ϕ.

Figure 2. Global distribution of landslides and their occupation status as of 2015. (a) Global overview of IPCC reference regions in this study: EAS, East Asia; MED, the Mediterranean; NEAF, Northeast Africa; NWS, North-Western South America; SEAF, Southeast Africa; TIB, the Tibetan Plateau; WCA, Central Asia; WCE, Western Central Europe; WNA, Western North America. Landslide and flood risk assessments were adapted from Adler et al. (2022). (b, c) Villages on a slow-moving landslide in the Poqueira Valley, Spain. (d, e) Slow-moving Pampahasi landslide embedded in La Paz, Bolivia. Global outline in panel (a) is from NaturalEarth, and mountain regions in dark gray from the Global Mountain Biodiversity Assessment (V2). Source of base maps in panels (c–e): Google Earth Imagery, 2014. Photograph in panel (c) by Reyes-Carmona, Granada, Spain.

We explore different processes that we assume to influence exposure in the forms the fraction inhabited of landslides in a basin, and the relative area of settlements on landslides. To this extent, we used different sets to estimate the parameters of the Bernoulli distribution (γ) and for the beta distribution (ϕ and γ) with regression models.

We then looked at the fraction of inhabited landslides in a basin with inhabited areas. In this model, each observation refers to a drainage basin that is labeled by the appropriate IPCC region. We estimated the response of the fraction of inhabited landslides inhabited to standardized basin characteristics as linear predictors describing degree of urbanization (*urb*), mean steepness (*stp*) and flood exposure (*flo*) to predict γ:

$$logit(\gamma_i) = \sum_{j=1}^{J} \alpha_{j_i} + \beta_{stp[j_i]}x_{stp[i]} + \beta_{urb[j_i]}\left(\beta_{stp*urb[i]}x_{stp[i]} + x_{urb[i]}\right) + \beta_{flo[j_i]}x_{flo[i]} \qquad (3)$$

where the intercepts, *a*, and model coefficients β, are composed of the pooled effect and regional effects. $x_{\mathrm{var}[j,i]}$ denotes respective observations of the predictor variables for the corresponding variable *var* in the corresponding regions for $j = 1, \ldots, J$, where $J = 9$ IPCC regions. We introduce an interaction coefficient $\beta_{stp*urb}$ in the prediction of γ, following an anticipation of a negative relationship between steeper basins and larger degrees of urbanization. The regional interaction coefficients show no credible influence and are reported in Table S2 in Supporting Information S1.

In reporting our results, we derived a posterior fraction by taking our models estimates (γ) and transforming this from log-odds to a percentage form through the *logit* function. Hence, we reported our estimates in the form of the average percentage landslides in a basin inhabited. Furthermore, the posterior coefficients are the log-odds of the response to marginal effects, where positive values indicate an increase in the fraction of inhabited landslides and negative values show a decrease. Formally, the odds ratio is a multiplicative factor describing the predicted probability of a landslide being occupied rather than unoccupied. This odds ratio can be calculated from the posterior coefficients (β) simply as e^{β}. We analyzed the odds ratios of observing an inhabited landslide in response to a marginal increase of one standard deviation in either urbanization (2% in area), steepness (11° in mean slope) or flood exposure (5% in area) of given basin, while keeping the other two variables at their means.

We also investigated how the presence of mapped slow-moving landslides and exposure to floods in basins across IPCC regions might affect the fraction of relative area of a landslide inhabited by permanent structures (Figure 1a). In this model, each observation ($Y_i > 0$) also corresponds to a drainage basin that is labeled by the appropriate IPCC region. In further using this model output in a hierarchical structure, we estimate the basin-averaged relative areas across IPCC regions.

We introduced slow-moving landslide density (*lan*) and flood exposure (*flo*) as linear predictors to the response of relative areas. The relative area values are on the continuous variables ranging between 0 and 1, and hence within the capabilities of the Beta distribution.

$$logit(\mu_i) = \sum_{j=1}^{J} \alpha_{j_i} + \beta_{lan[j_i]}x_{lan[i]} + \beta_{flo[j_i]}x_{flo[i]} \qquad (4)$$

$$\log(\phi_i) = \sum_{j=1}^{J} \alpha_{j_i} + \beta_{lan[j_i]}x_{lan[i]} + \beta_{flo[j_i]}x_{flo[i]} \qquad (5)$$

where a_{var} and β_{var} are composed of the pooled and regional effects for intercepts and coefficients corresponding to basin characteristics (*var*), respectively. $x_{\mathrm{var}[j,i]}$ denotes respective observations of the predictor variables for the corresponding variable *var* for the corresponding $j = 1, \ldots, J$ regions. In this model, we only predict the mean parameter μ of the beta distribution. Although the precision parameter ϕ is estimated during the inference, we do not consider it further.

A Bayesian approach requires a prior distribution for each parameter to be estimated. We encoded the absence of prior knowledge to characterize the drivers of slow-moving landslide exposure with wide symmetric priors used for Bayesian regression analysis instead of utilizing default (flat and improper) priors. We used weakly informative priors for pooled intercepts and standard deviations of coefficients across groups by assigning half Student-t prior distributions centered around 0, with 3 degrees of freedom, and a standard deviation of 2.5. In modeling the response of relative areas occupying a given slow-moving landslides at the population-level, we used Gaussian priors, centered at 0 with a standard deviation of 3, for the coefficients across all parameters of the Beta regression in Equations 4 and 5. Our choice of prior accommodates positive or negative responses of relative

area of settlements on slow-moving landslides to greater areas in a basin exposed to flooding or affected by slow-moving landslides (Figure 1a). We used Cauchy distributions as a weakly informative prior for the Bernoulli distribution in the Zero-inflated component (Gelman et al., 2008) in Equation 3, centered at zero and with a scale of 2.5. We used a Lewandowski-Kurowicka-Joe (LKJ) Cholesky correlation distribution as a prior for group-level effects to express uniform density over correlation matrices.

We standardized predictors across the database to increase the efficiency of the samples and improve numerical performance. This eases interpretation of the model intercepts as the expected target value if all predictors are at their average values. This also enables us to interpret credible deviations observed between posterior intercepts between the regional models from the pooled model.

We implemented a set-up of the Hamiltonian sampler in *brms*, using four parallel chains each with 3,500 samples after 1,000 warm-up runs. This resulted in total draws of 10,000. We observed $R_{hat} \leq 1.01$ in all runs, indicating stability chains in the numerical approximation. Model diagnostics and experiments with more samples showed that $\geq 2,000$ bulk and tail effective samples resulted in reliable estimates of a posterior distribution.

We used 90% credible intervals (CIs) to summarize the posterior distribution of parameters estimates across IPCC regions. We selected a 90% interval, that has 5% of the distribution on both sides beyond its limits that indicate the 5th and 95th percentiles. A 90% interval is computationally more stable than a 95% interval, which relies on only 2.5% of the posterior draws on its ends (Goodrich et al., 2024).

Furthermore, we assessed and compared regional posterior predictive estimates of median fractions of inhabited landslides and relative areas to those observed in our database, that were interpreted from the intercepts of the BEZI model (Figure S1 in Supporting Information S1). We evaluated the marginal influence of basin characteristics at one standard deviation from the mean across regions in Figure 5a. We illustrate that the marginal influence of each basin characteristic can vary for selected regions in Figures 5b–5d. Our model is most informed by observations about the 1 standard deviation from the global mean values, showing where the chance classifier deviates from marginal influence with the posterior predictive across each basin characteristic (Figure S2 in Supporting Information S1). We note our models' posterior predictions better follow the distribution of observed relative areas in IPCC regions informed by more inhabited landslide samples (Figure S3 in Supporting Information S1).

3. Results and Discussion

3.1. Human Settlements Exposed to Slow-Moving Landslides

Our database of 7,764 large slow-moving landslides is distributed across nine IPCC reference regions, assessed for future landslide and flood risk to people and infrastructure in the mountains (Adler et al., 2022). These IPCC regions represent areas of consistent climatic scenarios (Iturbide et al., 2020) (Figure 2). In five of these regions, landslide and flood risk levels could increase with global warming scenarios beyond 1.7°C; three regions are anticipated to remain unchanged. We located 1,134 landslides (15% of our database) in the Mediterranean (MED) and included this region in our study, although not assessed in the IPCC report on mountains. Four other IPCC regions that were assessed in this report (Adler et al., 2022) were not covered in our database.

We find a total settlement area of 55 km^2 on 563 landslides (7% of our database) in 2015 (Table S1 in Supporting Information S1). While the number of landslide samples per region differs from tens (SEAF, NEAF, and NWS) to thousands (EAS, MED, WCE, and WNA), we observe the most human settlements on landslides in MED (22 km^2), WCE (19 km^2) and EAS (5 km^2) (Figure S4 in Supporting Information S1). The most densely inhabited landslides are, on average, in NWS (33%) and SEAF (10%) with total settlement footprints covering 0.67 and 3.65 km^2, respectively.

Our pooled estimates across all IPCC regions show that 9_{-5}^{+16}% (median and 90% Credible Interval (CI)) of landslides mapped in a given basin are inhabited (Figure 3a). The only region that has a credibly differing estimate is EAS, where this fraction is lowest ($1_{-0.4}^{+0.4}$%). Regions such as SEAF, NEAF, NWS, and TIB have broad ranges of posterior estimates, but hardly stand out from the global average.
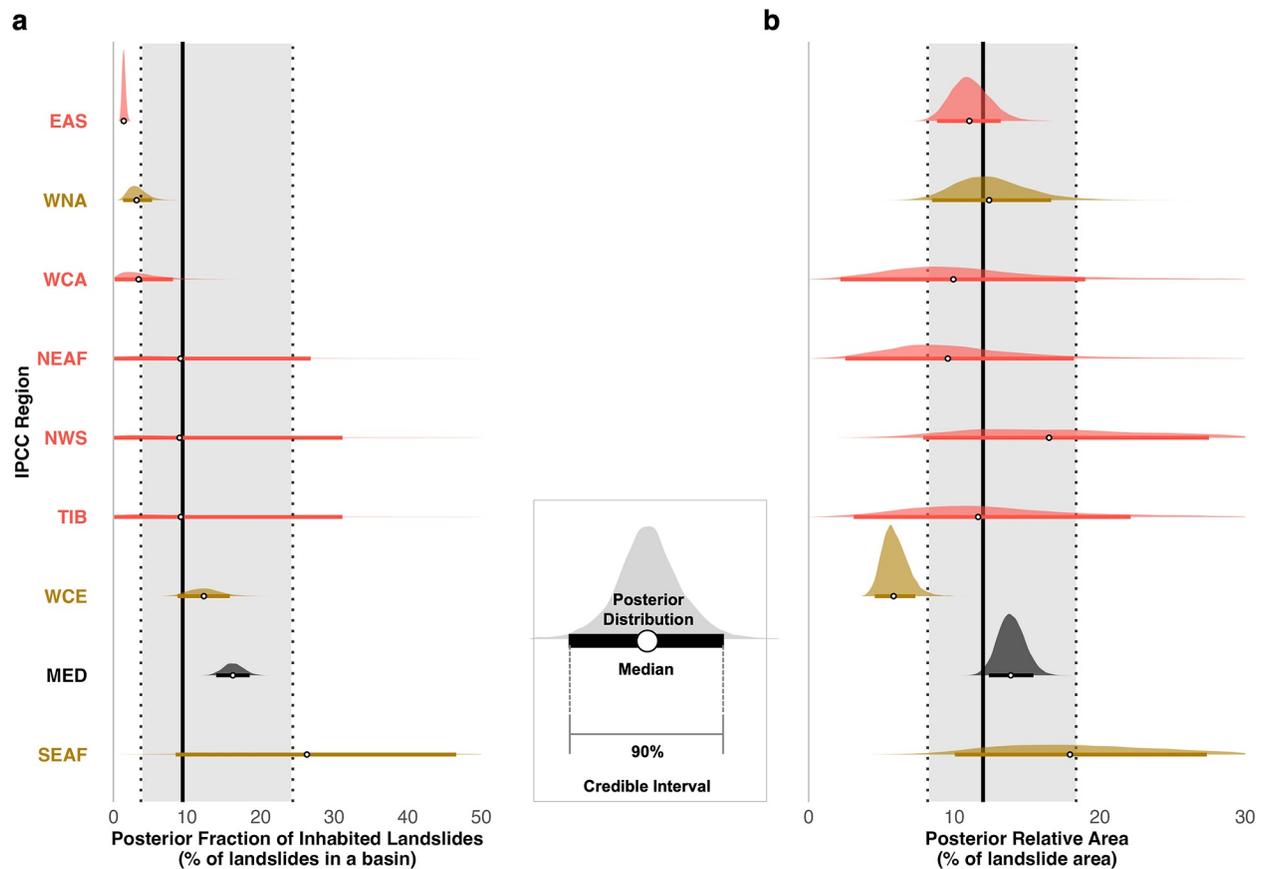
Figure 3. Estimates of posterior fraction of inhabited landslides in a basin and posterior relative area of settlements on landslides. (a) Posterior fraction of inhabited landslides in basins across IPCC regions. (b) Posterior relative areas in a basin across IPCC regions. Pooled estimates within a 90% Confidence Interval (CI) are shaded in gray and bounded by the black dotted lines, pooled median shown by a thick black line. The labels of IPCC regions are colored based on the projected change in landslide and flood risk in Figure 2.

Human settlement footprints occupy $12^{+7}_{-5}\%$ of a given landslide in our pooled model (Figure 3b). This fraction is lowest in WCE ($6^{+1}_{-1}\%$) and is credibly below the pooled estimate. Landslides are most densely occupied in NWS ($21^{+16}_{-14}\%$) and SEAF ($21^{+11}_{-12}\%$), on average. Narrow posterior distributions for WNA, EAS, and the MED partly reflect high regional sample sizes of >1,000 landslides.

3.2. Response of Settlement Areas to Floods and Landslides

The extent of human settlements on landslides credibly varies in response to flood exposure across regions (Figure 4a). We compared the linear responses of the relative area of landslides inhabited to the presence of mapped slow-moving landslides and the fraction flood-exposed area in their basins. The sign of the posterior predictor weights learned from our models were interpreted to distinguish between heightened and managed landslide exposure as a function the level of hazards present in basins across IPCC regions (Figure 1). We attribute *heightened exposure* from credible positive weights that indicate landslide exposure increases with the predictors describing flood exposure or the abundance of slow-moving landslides in a basin. Conversely, we attributed *managed exposure* to credibly negative weights.

Regionally, settlement footprints on landslides consistently tend to decrease with more mapped landslides in a given basin (Figure 4a). All regional posterior coefficients overlap with the pooled model and only WCE has a credibly negative range of estimates (Figure 4c). We observe that flood exposure raises relative areas of landslide inhabited by settlements from the pooled posterior coefficients (Figure 4b), but find diverging effects across IPCC regions (Figure 4d). Flood exposure credibly decreases the relative areas of settlements on landslides in EAS and WCE, but increases them in WNA and SEAF.
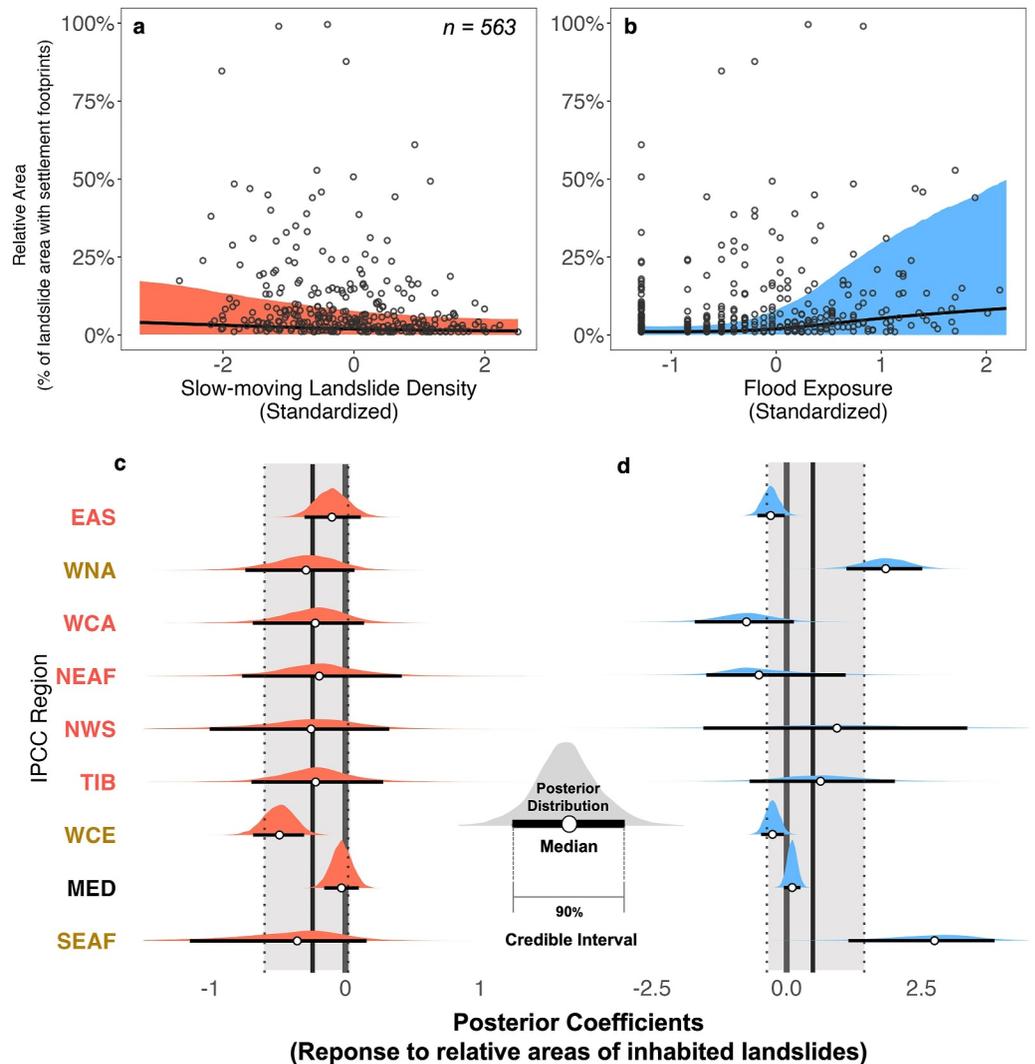
Figure 4. Responses of relative areas of settlements on landslides to the presence of slow-moving landslide and flood exposure in each basin. (a) Pooled response of relative areas to standardized slow-moving landslide density. (b) Pooled response of relative areas to standardized flood exposure. Shaded regions are the posterior predictive values within 90% credible intervals. Gray dots are the observed basin-averaged relative areas. (c) Regional posterior coefficients showing the model responses of relative areas to slow-moving landslide density, and, (d) show regional responses to flood exposure. Labels of IPCC regions are colored based on the projected change in landslide and flood risk in Figure 2. Pooled estimates shaded in gray are within a 90% Confidence Interval (CI) and bounded by the black dotted lines; pooled median shown by a thick black line.

3.3. Role of Basin Characteristics on Landslide Exposure

We surmise that the patterns of settlement footprints on slow-moving landslides reflect an interaction between human decisions to retain geographical benefits amid landslide-prone areas (Maes et al., 2019; Satterthwaite et al., 2007), establish settlements in settings limited by steep terrain (Forno et al., 2013; Omurakunova et al., 2020; Reyes-Carmona et al., 2023; Rusk et al., 2022), and avoid flood exposure (Devitt et al., 2023; Gong et al., 2021; Mård et al., 2018). Our model indicates that the fraction of landslides inhabited across IPCC regions grows with urbanization, except in WCA (Figure 5a). However, the influence of steeper basins is ambiguous and the response to flood exposure varies regionally. All three of our predictors have credible non-zero influences for EAS, WNA, WCE, and MED, while only urbanization has positive influence for SEAF, TIB, NEAF, NWS; neither of the basin characteristics have credible influence in WCA.
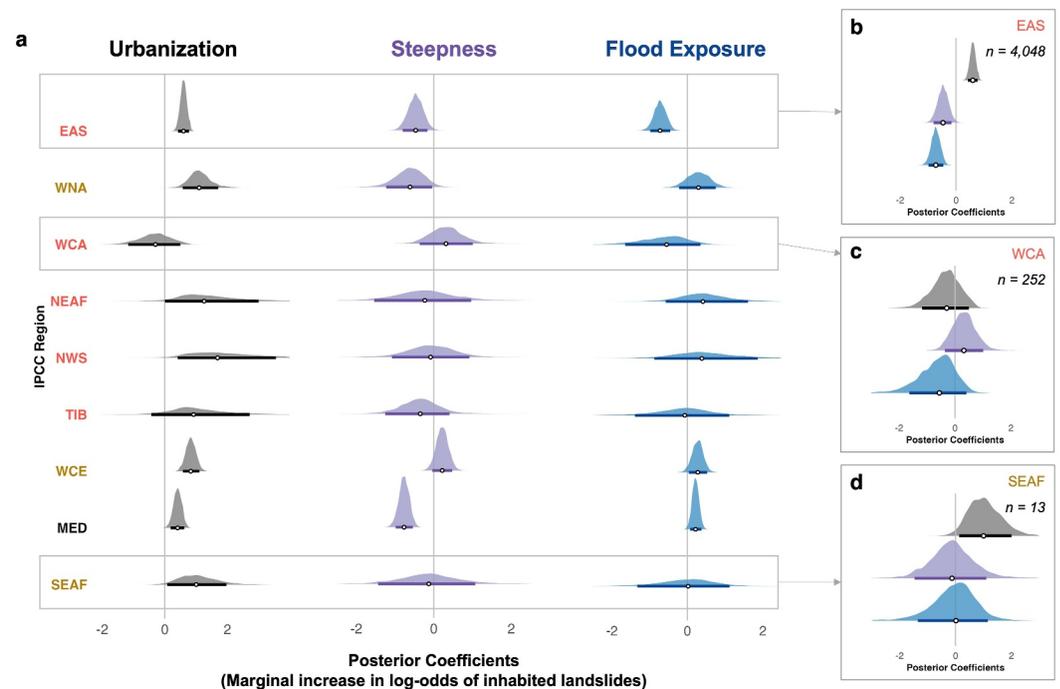
Figure 5. Regional variations in the posterior probability of inhabited landslides, and the marginal influences of urbanization, steepness, and inundation extent. (a) Regional posterior coefficients for urbanization, steepness, and flood exposure from the zero-inflated component of the Bayesian BEZI model corresponding to a marginal increase in each basin characteristic. (b) Regional posterior coefficients in East Asia (EAS), (c), Central Asia (WCA), and (d), Southeast Africa (SEAF). The labels of IPCC regions are colored based on the projected change in landslide and flood risk in Figure 2.

In EAS, posterior coefficients of urbanization, steepness, and flood exposure have credible non-zero influences on the fraction of landslides inhabited (Figure 5b). Urbanization increases the odds ratio of observing an inhabited landslide by $1.8^{+0.3}_{-0.3}$ times, for fixed steepness and flood exposure. In contrast, the odds ratio decreases by $0.6^{+0.2}_{-0.2}$ times with steeper terrain and by $0.5^{+0.1}_{-0.1}$ times in settings more exposed to flood, with all other predictors held constant. The posterior coefficients for WCA show that our selected basin characteristics are inconclusive in predicting the odds of observing an inhabited landslide (Figure 5c). In SEAF, only urbanization has a credible marginal influence to increase the odds by $2.9^{+6}_{-1.6}$ times (Figure 5d).

3.4. Exposure Responds to Floods Over Slow-Moving Landslides

Could the impact of flood exposure eclipse the hazard posed by slow-moving landslides? The extent of human settlements on large, slow-moving landslides might be a response to greater flood exposure than the reduced availability of stable terrain. Globally, we observe that flood exposure raises relative areas of settlements on landslides (Figure 4b). We infer a heightened landslide exposure (defined in Figure 1c) from the positive posterior coefficients in WNA and SEAF, and managed landslide exposure in EAS and WCE, which have negative posterior coefficients (Figure 4d). However, the relative area of settlements on landslides decreases with an abundance of mapped slow-moving landslides in a basin. Judging from the negative pooled posterior coefficients (Figure 4a) and across regions (Figure 4c), we infer managed exposure.

Our interpretation of managed exposure in East Asia might reflect how a combination of structural and nonstructural measures has been effective in mitigating negative impacts of landslides (Shinohara & Kume, 2022; H. Tang et al., 2019). Nearly half of our database consists of landslides from Japan, where up to 30% of the country's area is affected by upstream inundation from dams constructed since the 1980s (Itsukushima, 2023). Landslides in reservoir areas across Japan are subject to structural measures and enhanced erosion control facilities specified in legislation enacted in the mid-1900s (Shinohara & Kume, 2022). Nationwide efforts under the Sediment Disaster Prevention Act of 2000 (Junichi & Naoki, 2020) have further introduced measures to stabilize slopes to mitigate the impacts from deep-seated landslides, alongside early warning systems and evacuation plans.

Although our model from EAS is heavily informed by samples from Japan, reservoirs across China have similar landslide mitigation strategies and settlement relocation programs (Liu et al., 2021; H. Tang et al., 2019; Tomás et al., 2014; Zhang et al., 2018). For instance, a settlement in Badong County along the Yangtze River, China, was relocated between 1982 and 2003 due to construction of the Three Gorges Dam (Gong et al., 2021). However, the new settlement was placed on the Huangtupo landslide, which was reactivated with the beginning of reservoir operation (Tomás et al., 2014) and necessitated relocation (Gong et al., 2021). Relocation is costly and difficult to implement (Li et al., 2019; Wu et al., 2022), while retaining structures to stabilize a landslide (Zhang et al., 2018) can increase motion-drive damage due to subsurface alterations in the construction process (Ma et al., 2021). The managed exposure of EAS that we infer (Figure 5b) from the decrease of inhabited landslides in areas marginally more exposed to flooding and inundation may have resulted from this range of measures, monitoring, and regulations implemented across reservoirs.

3.5. Urban Population Pressure Influences Landslide Exposure

In most regions of our study, landslide exposure increases in more urbanized basins (Figure 5a). People that migrate from rural to urban areas in search of livelihoods, or fleeing conflict (Bachmann et al., 2019) may bring communities onto areas hosting slow-moving landslides. As an example from the city of Bukavu in the Democratic Republic of the Congo (SEAF), communities fleeing conflict between the 1990s–2010s built-up and expanded their settlements on the Funu landslide, despite a rate of deformation ranging 0.6–3 m y^{-1} (Dille et al., 2022).

Communities surrounding economic and urban centers may expand despite the hazard imposed by these landslides (Depicker et al., 2021). For instance, in La Paz, Bolivia (NWS), heavy rainfall in February of 2011 caused the Pampahasi landslide to fail ($\sim$1.5 km^2), destroying 1,000 homes, and displacing 6,000 people (Roberts et al., 2019). Yet, nearly half this landslide area was built-up in 2015 and a further expansion of structures by 2022 (Figure 6), despite evidence of continued post-failure creep.

Poverty may further drive communities onto high-hazard areas (Ozturk et al., 2022; Tuladhar et al., 2015). Unplanned and unregulated patterns of growth across the Hindu-Kush-Himalayas (TIB) have brought many informal communities into potentially unstable terrain (Rusk et al., 2022). Our estimates highlight stark differences in data availability and commensurate model precision in regions with limited samples (i.e., NEAF, NWS, SEAF, and TIB in Figure 3). These regions need more investment in landslide detection and mapping to avoid increasing vulnerable proportions of society unknowingly exposed to slow-moving landslides.

As demographics of mountain populations change, the needs of communities situated on landslides should be considered by monitoring efforts, early warning systems, and evacuation strategies (Godone et al., 2023). Emigration will lead to declining populations in mountain regions of Europe (WCE, MED) (Adler et al., 2022) and Japan (EAS) (Tsutsumi, 2021). WCE in particular, has more inhabited landslides found in steeper environments (Figure 5 and Figure S5 in Supporting Information S1). This out-migration reduces the rural population, and changes the demographics of remaining communities. Hence, leaving largely ageing populations (Lutz et al., 2008) with less mobility to escape from damaged structures and resist physical trauma (Pollock & Wartman, 2020) could be exposed on slow-moving landslides.

Communities are under pressure to find suitable areas to settle on amid steep terrain (Rusk et al., 2022). In Central Asia (WCA), inhabited landslides are in steeper basins (Figure 5c and Figure S5 in Supporting Information S1). Most landslides of WCA are in the Alai Range, Kyrgyzstan, where convex profiles created by rotational movements (Teshebaeva et al., 2019) provide benches along hillslopes that are suitable to accommodate villages (Forno et al., 2013; Reyes-Carmona et al., 2023). We show a tendency of inhabited landslides in WCA to decrease in steeper basins (Figure 5c). Major urban centers in Kyrgyzstan between valley floodplains and foothills (Omurakunova et al., 2020) indicate that built-up areas in WCA could be constrained by steep slopes.

4. Outlook on Future Slow-Moving Landslide Risk

This study identifies IPCC regions with mountain populations that are at an elevated risk of experiencing increased climate change-related impacts. With evidence indicating growing exposure will drive risk in mountain regions (Adler et al., 2022), communities may be exposed to unstable slopes with ambiguous responses to changes in surface and subsurface hydrology that accompany urbanization (Dille et al., 2022; Notti et al., 2015) or
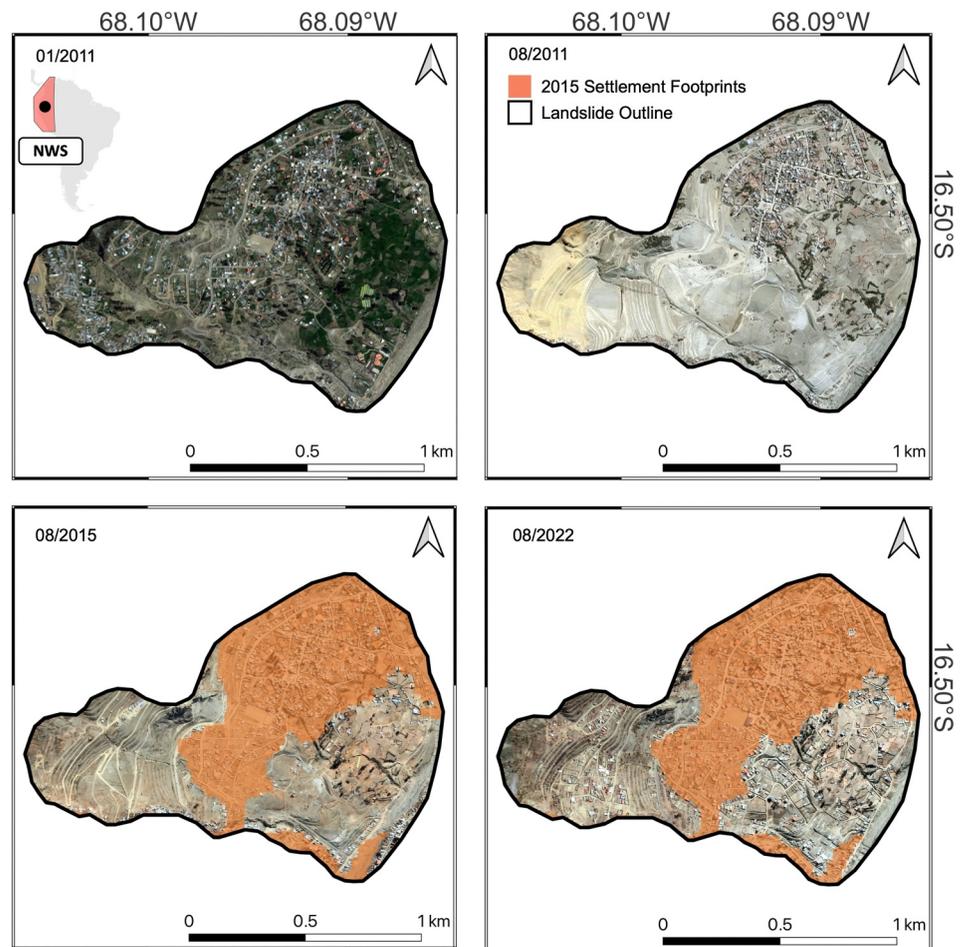
Figure 6. Satellite images of settlements on the Pampahasi urban landslide in La Paz, Bolivia, from 2011 to 2022 and the settlement footprints as of 2015. Source: Google Earth Imagery, 2011, 2015, and 2022.

acceleration from extreme weather accompanying changing climate conditions (Handwerger, Fielding, et al., 2019; Lacroix et al., 2020). However, there is considerable uncertainty regarding the extent to which these populations may be exposed to slow-moving landslides (Figure 3). In East Asia (EAS), landslide exposure credibly increases in more urbanized basins with gentler slopes, and less flood exposure (Figure 5b). In contrast, our estimates for the other IPCC regions facing growing landslide risk (Figure 2a) are least certain (i.e., for Northeast Africa (NEAF), Southeast Africa (SEAF), the Tibetan Plateau (TIB), and Central Asia (WCA)).

Countries within IPCC regions facing growing risk and with limited monitoring may need hundreds of landslides more to achieve assessments of exposure with credibility comparable to those in more monitored regions. Our findings indicate at least a thousand landslide samples per region give the most reliable estimates of exposure and their drivers (Figure 5a). The regional differences and limited landslide sample sizes in our database influence the widths of our estimates' credible intervals. To this end, our global assessment of exposure to slow-moving landslides not only illustrates, but also measures, how disparate knowledge creates largely differing levels of uncertainty.

The strength of our hierarchical model is that it offers an average perspective based on all available data on a near-global scale, with the advantage of highlighting regional deviations. Yet, it is the contrast between regional and global exposure that our model tries to capture. Here, the hierarchical framework helps to inform the models of regions with limited landslide data by learning from those with more data. We further argue that the Bayesian treatment of this problem makes the results as robust and credible as possible, given the available data. A natural refinement to our models would be to normalize sample size by the size per IPCC

region. However, IPCC regions include large areas without mountains or sufficient susceptibility to slow-moving landslides.

Growing flood hazards may outpace flood protection and displace communities, leading to migration away from flood-prone areas (Bachmann et al., 2019; Mård et al., 2018), thus, raising a risk of settlements expanding onto slow-moving landslides (Figure 4d). For instance, in the south of Italy, laws imposing building restrictions in floods-prone areas (Salvati et al., 2014) have led to an expansion into landslide-prone areas (Caleca et al., 2022). Despite constraints of sample size, we learn more about regional landslide exposure from our proxy of flood exposure than from slow-moving landslide density (Figures 4c and 4d). Evidence from our results leads us to emphasize that integrating landslide exposure, alongside flood risk assessments, in land use policy is crucial to manage relocation within mountain regions in the face of growing risks.

Our findings on the ambiguous role of catchment steepness on slow-moving landslide exposure (Figure 5a) warrant further inquiry into landslide exposure driven by the global expansion of urban land onto steeper slopes (Shi et al., 2023). Furthermore, competition between agricultural and urban land use has prompted uphill development (Zhou et al., 2021). Patterns of seasonal irrigation, characterized by the inundation data of this study (Dryden et al., 2021), could be used to investigate the influences of pressure from food security and agriculture on landslide exposure.

Future research looking into probable scenarios of failure mechanisms, and the likely areas impacted by catastrophically failing slow-moving landslides can provide a more comprehensive local understanding of exposure to communities and stakeholders. Our database is a compilation of heterogeneous types of slow-moving landslides in diverse geographical locations, and environments that could comprise multiple movements and complex failure mechanisms (Bhuyan et al., 2024). Populations, assets, and infrastructure in areas beyond slow-moving landslide areas may be exposed to down-slope impacts of catastrophic failure (Lacroix et al., 2020; Pánek & Klimeš, 2016), or up-slope to retrogressive failure (Bru et al., 2017). We recommend considering likely scenarios of failures to help stakeholders better assess their exposure to the cascading effects of specific landslides failure mechanisms posing a hazard to their communities.

We underline contrasts between well-monitored regions and those in demand of more landslide research. Four IPCC regions (South Asia, Southern Australasia, New Zealand, Northwestern North America) assessed for future mountain risks (Adler et al., 2022) are absent in our database. We emphasize that slow-moving landslides with settlements in these regions are present across New Zealand (Cook et al., 2022; Massey et al., 2016), Canada (Mansour et al., 2011), and India (Jain et al., 2024). Remote sensing workflows to expand systematic mapping of slow-moving landslides (Van Wyk de Vries et al., 2024) have the potential to strengthen the exposure assessments of data-scarce regions identified in our study. Our new database can be used for future assessments at different geographical scales or together with new inventories to inform populations, with uncertain slow-moving landslide exposure, that face a world with evolving risks.

Data Availability Statement

All codes and model data used for the statistical analysis and figures in the study are openly accessible and available at Zenodo via (Ferrer, 2024) (https://zenodo.org/records/12549429).

References

Adler, C., Wester, P., Bhatt, I., Huggel, C., Insarov, G., Morecroft, M., et al. (2022). Cross-chapter paper 5: Mountains. In H.-O. Pörtner, D. C. Roberts, M. Tignor, E. S. Poloczanska, K. Mintenbeck, A. Alegría, M. Craig, S. Langsdorf, S. Löschke, V. Möller, A. Okem, & B. Rama (Eds.), *Climate change 2022: Impacts, adaptation and vulnerability. Contribution of working group II to the sixth assessment report of the intergovernmental panel on climate change* (pp. 2273–2318). Cambridge University Press. https://doi.org/10.1017/9781009325844.022

Bachmann, F., Maharjan, A., Thieme, S., Fleiner, R., & Wymann von Dach, S. (2019). *Migration and sustainable mountain development: Turning challenges into opportunities. Bern, Switzerland: Centre for Development and Environment (CDE)*. University of Bern, with Bern with Bern Open Publishing (BOP).

Bellas, M., & Voulgaridis, G. (2018). Study of the major landslide at the community of Ropoto, Central Greece, mitigation and FBG early warning system design. *Innovative Infrastructure Solutions*, *3*(1), 30. https://doi.org/10.1007/s41062-018-0133-8

Bhuyan, K., Rana, K., Ferrer, J. V., Cotton, F., Ozturk, U., Catani, F., & Malik, N. (2024). Landslide topology uncovers failure movements. *Nature Communications*, *15*(1), 2633. https://doi.org/10.1038/s41467-024-46741-7

Bru, G., González, P. J., Mateos, R. M., Roldán, F. J., Herrera, G., Béjar-Pizarro, M., & Fernández, J. (2017). A-DInSAR Monitoring of Landslide and Subsidence Activity: A Case of Urban Damage in Arcos de la Frontera, Spain. *Remote Sensing*, *9*(8), 787. https://doi.org/10.3390/rs9080787

Bürkner, P.-C. (2017). Brms: An R package for Bayesian multilevel models using Stan. *Journal of Statistical Software*, *80*, 1–28. https://doi.org/10.18637/jss.v080.i01

Caleca, F., Tofani, V., Segoni, S., Raspini, F., Rosi, A., Natali, M., et al. (2022). A methodological approach of QRA for slow-moving landslides at a regional scale. *Landslides*, *19*(7), 1539–1561. https://doi.org/10.1007/s10346-022-01875-x

Chigira, M., Tsou, C.-Y., Matsushi, Y., Hiraishi, N., & Matsuzawa, M. (2013). Topographic precursors and geological structures of deep-seated catastrophic landslides caused by Typhoon Talas. *Geomorphology*, *201*, 479–493. https://doi.org/10.1016/j.geomorph.2013.07.020

Cignetti, M., Godone, D., Notti, D., Zucca, F., Meisina, C., Bordoni, M., et al. (2023). Damage to anthropic elements estimation due to large slope instabilities through multi-temporal A-DInSAR analysis. *Natural Hazards*, *115*(3), 2603–2632. https://doi.org/10.1007/s11069-022-05655-7

Cook, M. E., Brook, M. S., Hamling, I. J., Cave, M., Tunnicliffe, J. F., Holley, R., & Alama, D. J. (2022). Engineering geomorphological and InSAR investigation of an urban landslide, Gisborne, New Zealand. *Landslides*, *19*(10), 2423–2437. https://doi.org/10.1007/s10346-022-01938-z

Demurtas, V., Orrù, P. E., & Deiana, G. (2021). Deep-seated gravitational slope deformations in central Sardinia: Insights into the geomorphological evolution. *Journal of Maps*, *17*(2), 607–620. https://doi.org/10.1080/17445647.2021.1986157

Depicker, A., Jacobs, L., Mboga, N., Smets, B., Van Rompaey, A., Lennert, M., et al. (2021). Historical dynamics of landslide risk from population and forest-cover changes in the Kivu Rift. *Nature Sustainability*, *4*(11), 965–974. https://doi.org/10.1038/s41893-021-00757-9

Devitt, L., Neal, J., Coxon, G., Savage, J., & Wagener, T. (2023). Flood hazard potential reveals global floodplain settlement patterns. *Nature Communications*, *14*(1), 2801. https://doi.org/10.1038/s41467-023-38297-9

Dille, A., Dewitte, O., Handwerger, A. L., d'Oreye, N., Derauw, D., Ganza Bamulezi, G., et al. (2022). Acceleration of a large deep-seated tropical landslide due to urbanization feedbacks. *Nature Geoscience*, *15*(12), 1048–1055. https://doi.org/10.1038/s41561-022-01073-3

Dryden, R., Anand, M., Lehner, B., & Fluet-Chouinard, E. (2021). Do we prioritize floodplains for development and farming? Mapping global dependence and exposure to inundation. *Global Environmental Change*, *71*, 102370. https://doi.org/10.1016/j.gloenvcha.2021.102370

Emberson, R., Kirschbaum, D., & Stanley, T. (2020). New global characterisation of landslide exposure. *Natural Hazards and Earth System Sciences*, *20*(12), 3413–3424. https://doi.org/10.5194/nhess-20-3413-2020

Emberson, R., Kirschbaum, D., & Stanley, T. (2021). Global connections between El Nino and landslide impacts. *Nature Communications*, *12*(1), 2262. https://doi.org/10.1038/s41467-021-22398-4

Ferrari, S., & Cribari-Neto, F. (2004). Beta regression for modelling rates and proportions. *Journal of Applied Statistics*, *31*(7), 799–815. https://doi.org/10.1080/0266476042000214501

Ferrer, J. V. (2024). Supplementary data: Human settlement pressure drives slow-moving landslide exposure [Dataset]. *Zenodo*. https://doi.org/10.5281/zenodo.12549429

Fluet-Chouinard, E., Lehner, B., Rebelo, L.-M., Papa, F., & Hamilton, S. K. (2015). Development of a global inundation map at high spatial resolution from topographic downscaling of coarse-scale remote sensing data. *Remote Sensing of Environment*, *158*, 348–361. https://doi.org/10.1016/j.rse.2014.10.015

Forno, M. G., Gattiglio, M., Gianotti, F., Guerreschi, A., & Raiteri, L. (2013). Deep-seated gravitational slope deformations as possible suitable locations for prehistoric human settlements: An example from the Italian Western Alps. *Quaternary International*, *303*, 180–190. https://doi.org/10.1016/j.quaint.2013.03.033

Gelman, A. (2006). Multilevel (hierarchical) modeling: What it can and cannot do. *Technometrics*, *48*(3), 432–435. https://doi.org/10.1198/004017005000000661

Gelman, A., & Hill, J. (2006). *Data analysis using regression and multilevel/hierarchical models*. Cambridge university press.

Gelman, A., Jakulin, A., Pittau, M. G., & Su, Y.-S. (2008). A weakly informative default prior distribution for logistic and other regression models. *Annals of Applied Statistics*, *2*(4), 1360–1383. https://doi.org/10.1214/08-AOAS191

Gizzi, F. T., Bentivenga, M., Lasaponara, R., Danese, M., Potenza, M. R., Sileo, M., & Masini, N. (2019). Natural hazards, human factors, and "Ghost Towns": A multi-level approach. *Geoheritage*, *11*(4), 1533–1565. https://doi.org/10.1007/s12371-019-00377-y

Godone, D., Allasia, P., Notti, D., Baldo, M., Poggi, F., & Faccini, F. (2023). Coexistence of a marginal mountain community with large-scale and low kinematic landslide: The intensive monitoring approach. *Remote Sensing*, *15*(13), 3238. https://doi.org/10.3390/rs15133238

Gong, W., Juang, C. H., & Wasowski, J. (2021). Geohazards and human settlements: Lessons learned from multiple relocation events in Badong, China – Engineering geologist's perspective. *Engineering Geology*, *285*, 106051. https://doi.org/10.1016/j.enggeo.2021.106051

Goodrich, B., Gabry, J., Ali, I., & Brilleman, S. (2024). Rstanarm: Bayesian applied regression modeling via Stan.

Handwerger, A. L., Fielding, E. J., Huang, M.-H., Bennett, G. L., Liang, C., & Schulz, W. H. (2019). Widespread initiation, reactivation, and acceleration of landslides in the northern California coast ranges due to extreme rainfall. *Journal of Geophysical Research: Earth Surface*, *124*(7), 1782–1797. https://doi.org/10.1029/2019JF005035

Handwerger, A. L., Fielding, E. J., Sangha, S. S., & Bekaert, D. P. S. (2022). Landslide sensitivity and response to precipitation changes in wet and dry climates. *Geophysical Research Letters*, *49*(13), e2022GL099499. https://doi.org/10.1029/2022GL099499

Handwerger, A. L., Huang, M.-H., Fielding, E. J., Booth, A. M., & Bürgmann, R. (2019). A shift from drought to extreme rainfall drives a stable landslide to catastrophic failure. *Scientific Reports*, *9*(1), 1569. https://doi.org/10.1038/s41598-018-38300-0

Haque, U., da Silva, P. F., Devoli, G., Pilz, J., Zhao, B., Khaloua, A., et al. (2019). The human cost of global warming: Deadly landslides and their triggers (1995–2014). *Science of the Total Environment*, *682*, 673–684. https://doi.org/10.1016/j.scitotenv.2019.03.415

Herrera, G., Gutiérrez, F., García-Davalillo, J. C., Guerrero, J., Notti, D., Galve, J. P., et al. (2013). Multi-sensor advanced DInSAR monitoring of very slow landslides: The Tena Valley case study (Central Spanish Pyrenees). *Remote Sensing of Environment*, *128*, 31–43. https://doi.org/10.1016/j.rse.2012.09.020

Hungr, O., Leroueil, S., & Picarelli, L. (2014). The Varnes classification of landslide types, an update. *Landslides*, *11*(2), 167–194. https://doi.org/10.1007/s10346-013-0436-y

Itsukushima, R. (2023). Historical development and the present status of Japanese dams. *River Research and Applications*, *39*(6), 1136–1147. https://doi.org/10.1002/rra.4129

Iturbide, M., Gutiérrez, J. M., Alves, L. M., Bedia, J., Cerezo-Mota, R., Cimadevilla, E., et al. (2020). An update of IPCC climate reference regions for subcontinental analysis of climate model data: Definition and aggregated datasets. *Earth System Science Data*, *12*(4), 2959–2970. https://doi.org/10.5194/essd-12-2959-2020

Jain, N., Roy, P., Jalan, P., Martha, T. R., & Das, I. C. (2024). Irshalwadi landslide in Western Ghats of India: Observations from precursory slope movement, rainfall and soil moisture. *Natural Hazards Research*. https://doi.org/10.1016/j.nhres.2024.01.004

Junichi, K., & Naoki, I. (2020). Outline of measures for sediment disaster by the Sabo department of MLIT, Japan. *Landslides*, *17*(11), 2503–2513. https://doi.org/10.1007/s10346-020-01554-9

Lacroix, P., Handwerger, A. L., & Bièvre, G. (2020). Life and death of slow-moving landslides. *Nature Reviews Earth & Environment*, *1*(8), 404–419. https://doi.org/10.1038/s43017-020-0072-8

Lehner, B., Messager, M. L., Korver, M. C., & Linke, S. (2022). Global hydro-environmental lake characteristics at high spatial resolution. *Scientific Data*, *9*(1), 351. https://doi.org/10.1038/s41597-022-01425-z

Li, D., Yan, L., Wu, L., Yin, K., & Leo, C. (2019). The Hejiapingzi landslide in Weining county, Guizhou Province, southwest China: A recent slow-moving landslide triggered by reservoir drawdown. *Landslides*, *16*(7), 1353–1365. https://doi.org/10.1007/s10346-019-01189-5

Lin, Q., Steger, S., Pittore, M., Zhang, Y., Zhang, J., Zhou, L., et al. (2023). Contrasting population projections to induce divergent estimates of landslides exposure under climate change. *Earth's Future*, *11*(9), e2023EF003741. https://doi.org/10.1029/2023EF003741

Linke, S., Lehner, B., Ouellet Dallaire, C., Ariwi, J., Grill, G., Anand, M., et al. (2019). Global hydro-environmental sub-basin and river reach characteristics at high spatial resolution. *Scientific Data*, *6*(1), 283. https://doi.org/10.1038/s41597-019-0300-6

Liu, X., Zhao, C., Zhang, Q., Yin, Y., Lu, Z., Samsonov, S., et al. (2021). Three-dimensional and long-term landslide displacement estimation by fusing C- and L-band SAR observations: A case study in Gongjue county, Tibet, China. *Remote Sensing of Environment*, *267*, 112745. https://doi.org/10.1016/j.rse.2021.112745

Lutz, W., Sanderson, W., & Scherbov, S. (2008). The coming acceleration of global population ageing. *Nature*, *451*(7179), 716–719. https://doi.org/10.1038/nature06516

Ma, P., Cui, Y., Wang, W., Lin, H., & Zhang, Y. (2021). Coupling InSAR and numerical modeling for characterizing landslide movements under complex loads in urbanized hillslopes. *Landslides*, *18*(5), 1611–1623. https://doi.org/10.1007/s10346-020-01604-2

Maes, J., Molombe, J. M., Mertens, K., Parra, C., Poesen, J., Che, V. B., & Kervyn, M. (2019). Socio-political drivers and consequences of landslide and flood risk zonation: A case study of Limbe city, Cameroon. *Environment and Planning C: Politics and Space*, *37*(4), 707–731. https://doi.org/10.1177/2399654418790767

Maki Mateso, J.-C., Dewitte, O., & Bielders, C. L. (2024). Living with landslides: Land use on unstable hillslopes in a rural tropical mountainous environment in DR Congo. *Science of the Total Environment*, *925*, 171624. https://doi.org/10.1016/j.scitotenv.2024.171624

Mansour, M. F., Morgenstern, N. R., & Martin, C. D. (2011). Expected damage from displacement of slow-moving slides. *Landslides*, *8*(1), 117–131. https://doi.org/10.1007/s10346-010-0227-7

Marconcini, M., Metz-Marconcini, A., Üreyen, S., Palacios-Lopez, D., Hanke, W., Bachofer, F., et al. (2020). Outlining where humans live, the world settlement footprint 2015. *Scientific Data*, *7*(1), 242. https://doi.org/10.1038/s41597-020-00580-5

Mård, J., Di Baldassarre, G., & Mazzoleni, M. (2018). Nighttime light data reveal how flood protection shapes human proximity to rivers. *Science Advances*, *4*(8), eaar5779. https://doi.org/10.1126/sciadv.aar5779

Massey, C. I., Petley, D. N., McSaveney, M. J., & Archibald, G. (2016). Basal sliding and plastic deformation of a slow, reactivated landslide in New Zealand. *Engineering Geology*, *208*, 11–28. https://doi.org/10.1016/j.enggeo.2016.04.016

McElreath, R. (2018). *Statistical rethinking: A Bayesian course with examples in R and Stan*. Chapman and Hall/CRC.

Nadim, F., Kjekstad, O., Peduzzi, P., Herold, C., & Jaedicke, C. (2006). Global landslide and avalanche hotspots. *Landslides*, *3*(2), 159–173. https://doi.org/10.1007/s10346-006-0036-1

Nardi, F., Annis, A., Di Baldassarre, G., Vivoni, E. R., & Grimaldi, S. (2019). GFPLAIN250m, a global high-resolution dataset of Earth's floodplains. *Scientific Data*, *6*(1), 180309. https://doi.org/10.1038/sdata.2018.309

Notti, D., Galve, J. P., Mateos, R. M., Monserrat, O., Lamas-Fernández, F., Fernández-Chacón, F., et al. (2015). Human-induced coastal landslide reactivation. Monitoring by PSInSAR techniques and urban damage survey (SE Spain). *Landslides*, *12*(5), 1007–1014. https://doi.org/10.1007/s10346-015-0612-3

Omurakunova, G., Bao, A., Xu, W., Duulatov, E., Jiang, L., Cai, P., et al. (2020). Expansion of impervious surfaces and their driving forces in highly urbanized cities in Kyrgyzstan. *International Journal of Environmental Research and Public Health*, *17*(1), 362. https://doi.org/10.3390/ijerph17010362

Ospina, R., & Ferrari, S. L. P. (2010). Inflated beta distributions. *Statistical Papers*, *51*(1), 111–126. https://doi.org/10.1007/s00362-008-0125-4

Ozturk, U., Bozzolan, E., Holcombe, E. A., Shukla, R., Pianosi, F., & Wagener, T. (2022). How climate change and unplanned urban sprawl bring more landslides. *Nature*, *608*(7922), 262–265. https://doi.org/10.1038/d41586-022-02141-9

Pánek, T., & Klimeš, J. (2016). Temporal behavior of deep-seated gravitational slope deformations: A review. *Earth-Science Reviews*, *156*, 14–38. https://doi.org/10.1016/j.earscirev.2016.02.007

Pelascini, L., Steer, P., Mouyen, M., & Longuevergne, L. (2022). Finite-hillslope analysis of landslides triggered by excess pore water pressure: The roles of atmospheric pressure and rainfall infiltration during typhoons. *Natural Hazards and Earth System Sciences*, *22*(10), 3125–3141. https://doi.org/10.5194/nhess-22-3125-2022

Pollock, W., & Wartman, J. (2020). Human vulnerability to landslides. *GeoHealth*, *4*(10), e2020GH000287. https://doi.org/10.1029/2020GH000287

Reyes-Carmona, C., Galve, J. P., Pérez-Peña, J. V., Moreno-Sánchez, M., Alfonso-Jorde, D., Ballesteros, D., et al. (2023). Improving landslide inventories by combining satellite interferometry and landscape analysis: The case of Sierra Nevada (Southern Spain). *Landslides*, *20*(9), 1815–1835. https://doi.org/10.1007/s10346-023-02071-1

Roberts, N. J., Rabus, B. T., Clague, J. J., Hermanns, R. L., Guzmán, M.-A., & Minaya, E. (2019). Changes in ground deformation prior to and following a large urban landslide in La Paz, Bolivia, revealed by advanced InSAR. *Natural Hazards and Earth System Sciences*, *19*(3), 679–696. https://doi.org/10.5194/nhess-19-679-2019

Robinson, N., Regetz, J., & Guralnick, R. P. (2014). EarthEnv-DEM90: A nearly-global, void-free, multi-scale smoothed, 90m digital elevation model from fused ASTER and SRTM data. *ISPRS Journal of Photogrammetry and Remote Sensing*, *87*, 57–67. https://doi.org/10.1016/j.isprsjprs.2013.11.002

Rusk, J., Maharjan, A., Tiwari, P., Chen, T.-H. K., Shneiderman, S., Turin, M., & Seto, K. C. (2022). Multi-hazard susceptibility and exposure assessment of the Hindu Kush Himalaya. *Science of the Total Environment*, *804*, 150039. https://doi.org/10.1016/j.scitotenv.2021.150039

Salvati, P., Bianchi, C., Fiorucci, F., Giostrella, P., Marchesini, I., & Guzzetti, F. (2014). Perception of flood and landslide risk in Italy: A preliminary analysis. *Natural Hazards and Earth System Sciences*, *14*(9), 2589–2603. https://doi.org/10.5194/nhess-14-2589-2014

Satterthwaite, D., Huq, S., Pelling, M., Reid, H., & Lankao, P. R. (2007). *Adapting to climate change in urban areas: The possibilities and constraints in low- and middle-income nations*. IIED.

Schoppa, L., Sieg, T., Vogel, K., Zöller, G., & Kreibich, H. (2020). Probabilistic flood loss models for companies. *Water Resources Research*, *56*(9), e2020WR027649. https://doi.org/10.1029/2020WR027649

Schulz, W. H., Kean, J. W., & Wang, G. (2009). Landslide movement in southwest Colorado triggered by atmospheric tides. *Nature Geoscience*, *2*(12), 863–866. https://doi.org/10.1038/ngeo659

Shi, K., Cui, Y., Liu, S., & Wu, Y. (2023). Global urban land expansion tends to be slope climbing: A remotely sensed nighttime light approach. *Earth's Future*, *11*(4), e2022EF003384. https://doi.org/10.1029/2022EF003384

Shinohara, Y., & Kume, T. (2022). Changes in the factors contributing to the reduction of landslide fatalities between 1945 and 2019 in Japan. *Science of the Total Environment*, *827*, 154392. https://doi.org/10.1016/j.scitotenv.2022.154392

Solari, L., Raspini, F., Del Soldato, M., Bianchini, S., Ciampalini, A., Ferrigno, F., et al. (2018). Satellite radar data for back-analyzing a landslide event: The Ponzano (Central Italy) case study. *Landslides*, *15*(4), 773–782. https://doi.org/10.1007/s10346-018-0952-x

Sundriyal, Y., Kumar, V., Chauhan, N., Kaushik, S., Ranjan, R., & Punia, M. K. (2023). Brief communication: The northwest Himalaya towns slipping towards potential disaster. *Natural Hazards and Earth System Sciences*, *23*(4), 1425–1431. https://doi.org/10.5194/nhess-23-1425-2023

Tang, B., Frye, H. A., Gelfand, A. E., & Silander, J. A. (2023). Zero-inflated beta distribution regression modeling. *Journal of Agricultural, Biological, and Environmental Statistics*, *28*(1), 117–137. https://doi.org/10.1007/s13253-022-00516-z

Tang, H., Wasowski, J., & Juang, C. H. (2019). Geohazards in the three Gorges reservoir area, China – Lessons learned from decades of research. *Engineering Geology*, *261*, 105267. https://doi.org/10.1016/j.enggeo.2019.105267

Team RC. (2023). *R: A language and environment for statistical computing*. R Foundation for Statistical Computing.

Team SD. (2023). Stan modeling language users guide and reference manual, version 2.26.1.

Teshebaeva, K., Echtler, H., Bookhagen, B., & Strecker, M. (2019). Deep-seated gravitational slope deformation (DSGSD) and slow-moving landslides in the southern Tien Shan Mountains: New insights from InSAR, tectonic and geomorphic analysis. *Earth Surface Processes and Landforms*, *44*(12), 2333–2348. https://doi.org/10.1002/esp.4648

Thornton, J. M., Snethlage, M. A., Sayre, R., Urbach, D. R., Viviroli, D., Ehrlich, D., et al. (2022). Human populations in the world's mountains: Spatio-temporal patterns and potential controls. *PLoS One*, *17*(7), e0271466. https://doi.org/10.1371/journal.pone.0271466

Tomás, R., Li, Z., Liu, P., Singleton, A., Hoey, T., & Cheng, X. (2014). Spatiotemporal characteristics of the Huangtupo landslide in the Three Gorges region (China) constrained by radar interferometry. *Geophysical Journal International*, *197*(1), 213–232. https://doi.org/10.1093/gji/ggu017

Tsutsumi, K. (2021). Depopulation as a regional problem and reality of depopulation. In K. Tsutsumi (Ed.), *Depopulation, aging, and living environments: Learning from social capital and mountainous areas in Japan* (pp. 17–58). Springer. https://doi.org/10.1007/978-981-15-9042-9_2

Tuladhar, G., Yatabe, R., Dahal, R. K., & Bhandary, N. P. (2015). Disaster risk reduction knowledge of local people in Nepal. *Geoenvironmental Disasters*, *2*(1), 5. https://doi.org/10.1186/s40677-014-0011-4

United Nations, Department of Economic and Social Affairs, Population Division. (2019). *World urbanization prospects: The 2018 revision (Tech. Rep.)*. United Nations.

Van Wyk de Vries, M., Arrell, K., Basyal, G. K., Densmore, A. L., Dunant, A., Harvey, E. L., et al. (2024). Detection of slow-moving landslides through automated monitoring of surface deformation using Sentinel-2 satellite imagery. *Earth Surface Processes and Landforms*, *49*(4), 1397–1410. https://doi.org/10.1002/esp.5775

Wu, M., Yi, X., Dun, J., Yang, J., Cai, W., & Zhang, G. (2022). Understanding the slow motion of the Wangjiashan landslide in the Baihetan reservoir area (China) from space-borne radar observations. *Advances in Civil Engineering*, *2022*(1), e1766038. https://doi.org/10.1155/2022/1766038

Zhang, Y., Meng, X., Jordan, C., Novellino, A., Dijkstra, T., & Chen, G. (2018). Investigating slow-moving landslides in the Zhouqu region of China using InSAR time series. *Landslides*, *15*(7), 1299–1315. https://doi.org/10.1007/s10346-018-0954-8

Zhou, L., Dang, X., Mu, H., Wang, B., & Wang, S. (2021). Cities are going uphill: Slope gradient analysis of urban expansion and its driving factors in China. *Science of the Total Environment*, *775*, 145836. https://doi.org/10.1016/j.scitotenv.2021.145836